ISIJ International, Vol. 55 (2015), No. 1, pp. 264–271

Liquid-Metal-Induced Embrittlement Related Microcrack Propagation on Zn-coated Press Hardening Steel

Chang Wook LEE,[1)] Won Seok CHOI,[1)] Lawrence CHO,[1)] Yeol Rae CHO[2)] and Bruno Charles De COOMAN[1)]*

1) Graduate Institute of Ferrous Technology, Pohang University of Science and Technology, 790-784, Pohang, South Korea.
2) POSCO Technical Research Laboratories, 545-090, Gwangyang, South Korea.

(*Received on June 10, 2014; accepted on September 17, 2014*)

The coatings on press hardening steel are needed to suppress high temperature oxidation and decarburization. Additional corrosion protection is provided by Zn coatings which provide cathodic protection to press hardened parts. Due to the low melting temperature of Zn and Zn–Fe intermetallic compounds, the Zn-coated PHSs are susceptible to LMIE during the die-quenching process. In the present work, the mechanical properties of Zn coated PHS were evaluated in terms of tensile properties and bending properties. A deterioration of the room temperature bendability, due to microcrack formation and propagation, was observed. The presence of Γ-Fe_3Zn_{10} observed in the microcracks at room temperature correspond to liquid Zn at the die-quenching temperature, making it possible to trace the progress of the liquid Zn phase during microcrack formation. The results suggest that Zn-grain boundary diffusion causes the phase transformation to ferrite of the austenite grain boundary region. This results in intergranular cracking due to the lower strength of ferrite. The LMIE microcrack formation is most severe in areas where the applied stress and the friction are highest during the forming process, making the occurrence of LMIE-mitigated microcrack propagation dependent on the local deformation conditions.

KEY WORDS: Press Hardening Steel (PHS); liquid metal induced embrittlement (LMIE); microcrack; Zn coating.

1. Introduction

The demands for the reduction of fuel consumption and increase of passenger safety has resulted in a increased the use of ultra-high strength steel for structural parts of passenger vehicles.[1)] Various high strength steel grades have been developed industrially for this purpose in the last decade such as dual-phase (DP), complex-phase (CP), transformation induced plasticity (TRIP), twinning induced plasticity (TWIP) and martensitic ultra-high strength steel.[2–6)] However, the use of high and ultra-high strength steel in press forming requires higher forming forces and often results in a large spring back effect.[7)] The press hardening process is the most efficient method to produce ultra-strength steel with a reduced or no spring back. The actual forming is carried out at high temperature and the spring back is significantly reduced because the strength of the material is typically only 150–200 MPa at high temperatures. The elongations is also considerable, typically 40% at the forming temperature.[8,9)] During the die-quenching in the direct press hardening process method the sheets are heated and simultaneously formed and die-quenched. The material is heated above the A_3 temperature to the austenite stability range and the forming and quenching carried out in water-cooled dies. During quenching the austenite-to-martensite phase transformation occurs. This phase transformation results in the formation of an untempered lath martensite microstructure with a 1 GPa yield strength (YS) and a 1.5 GPa ultimate tensile strength (UTS).[10)] These ultra-high strength properties, make press hardened steel parts ideally suited for anti-intrusion parts of passenger vehicles such as B-pillar reinforcements, bumper beams, cross beams and roof rails.[6)]

The 22MnB5 PHS grade is currently the most widely used material for the production of press hardened parts. The main alloying elements of 22MnB5 are C, Mn and B which increase the hardenability by retarding ferrite formation during austenite decomposition.[11)] Ti is added to suppress the formation of BN and Cr additions are made to increase the hardenability. To ensure the formation of a fully martensitic microstructure after the press hardening process, the cooling rate should typically be higher than $-25°Cs^{-1}$.[12)] The use of a coated rather than an uncoated PHS is aimed at preventing oxidation and surface decarburization. The most widely used coating is currently the Al-10%Si alloy coating which provides excellent barrier protection.[9)] This coating also provides some sacrificial corrosion protection, which is generally considered to be insufficient.[13)] With increasing customer expectations with regard to cosmetic and perforation corrosion, providing coated PHSs with additional cathodic protection has become a major issue. Zn and Zn-alloyed coating are therefore being developed.[14,15)] However, the formation of small surface cracks on die-quenched Zn-coated PHS panels related to liquid metal induced embrittlement (LMIE), has been widely reported.[8)] Because of the low melting temperature of Zn and Fe–Zn intermetal-

* Corresponding author: E-mail: decooman@postech.ac.kr
DOI: http://dx.doi.org/10.2355/isijinternational.55.264

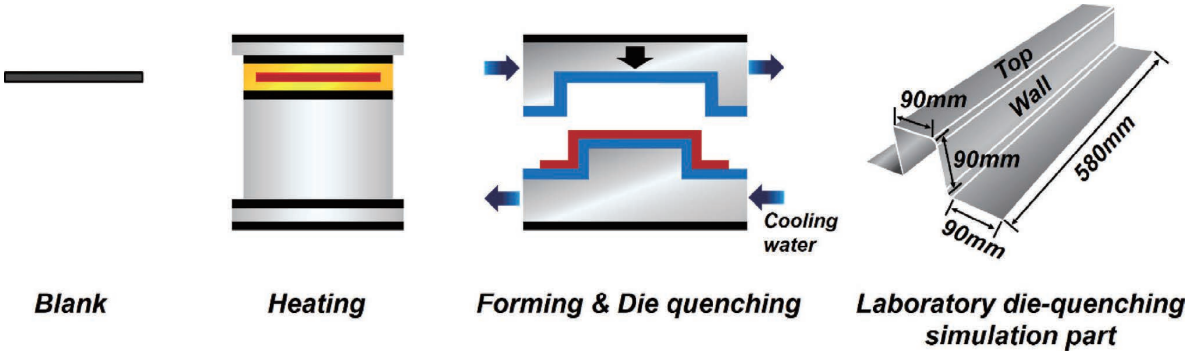

Fig. 1. Schematic of the press hardening process and geometry of the die-quenched parts used in the present work.

lic compounds, most of the Zn and Zn-alloy coatings are partially liquid at the austenitizing temperature. If sufficient stress is applied during the forming operation at high temperature, a Fe-saturated liquid Zn, appears to penetrate into the austenite grain boundaries causing an embrittlement characterized by surface crack formation due to a rapid intergranular fracture. Lee *et al*. suggested that the susceptibility of LMIE could be reduced by eliminating the presence of the liquid Zn phase by a diffusion annealing treatment involving longer soaking times, a higher heating temperature or the use of thinner coatings.[8] The formation of LMIE surface cracks is particularly pronounced in those parts of the press formed parts which have been exposed to deformation in high friction areas during die quenching. Drillet *et al*. reported that the microcrack propagation was related to the high temperature friction between the coating and tool surfaces.[16]

The cracks do not cause the full catastrophic fracture of the part during die quenching. Instead mostly surface microcracks are formed. These cracks may however impact the mechanical behaviour of PHS parts negatively. The most important mechanical properties for crash performance of structural automotive parts, especially PHS, are tensile strength and bending performance. In the case of PHS, the tensile properties are directly related to the intrinsic strength of the low C lath martensite microstructure. A clear relationship between the outcome of full-scale crash tests and the bendability of PHS was reported by Till *et al*.[17] and Manuel *et al*.[18]

As there are clear indications that the bending performance of materials is affected by the local surface microstructure,[19] the mechanical properties of the die quenched Zn-coated 22MnB5 PHS grade were investigated in the present work to verify the relation between the deterioration of the bending performance and the LMIE microcrack propagation.

2. Experimental

A 22MnB5 (Fe-0.21%C-1.23%Mn-0.002%B in mass%) PHS grade was prepared by vacuum induction melting (VIM) and the ingots were hot rolled and cold rolled to a final thickness of 1.5 mm. The full hard cold rolled panels were hot-dip galvanized in a laboratory galvanizing simulator. The temperature of the Fe-saturated Zn-0.12 mass% Al hot dip galvanizing bath was kept at 450°C, and the dipping time was fixed at 5 seconds. The thickness of the Zn coating

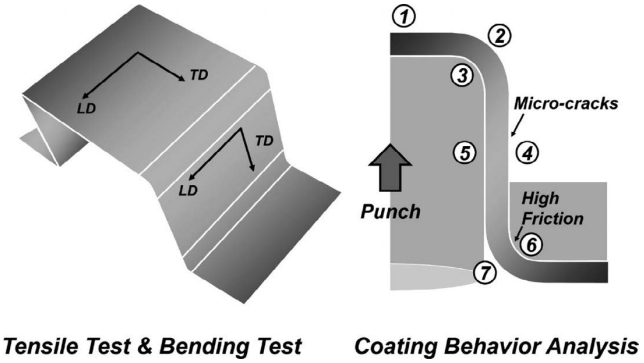

Fig. 2. Schematics showing where specimens were taken for the mechanical tests and the microanalysis.

on the PHS was approximately 10 μm. Uncoated 22MnB5 PHS was used as reference material to investigate the effect of the Zn coating on the mechanical properties.

The direct press hardening process which was used for the Zn-coated 22MnB5 PHS part in the course of the present work is illustrated in **Fig. 1**. A steel blank was heated to 900°C to get a fully austenitic microstructure. The heating rate was 5°Cs^{-1} and a holding time of about 2 min was selected to homogenise the temperature of the steel blanks. The blank was transferred to a die quenching press, formed into a hat-shaped channel at 750°C and simultaneously quenched by water cooled dies with cooling rate of –70°Cs^{-1}. The dimensions of the part are shown in Fig. 1.

Specimens used to determine the mechanical properties of the different segments of the die-quenched part were taken from the part as shown in **Fig. 2**. The tests consisted of tensile tests and three-point bending tests. The specimens were prepared in the direction parallel to the length direction (LD) of the die-quenching channel and in the transverse direction (TD). ASTM E8 type tensile specimens were prepared for the LD-oriented samples. Due to the part dimensions, the TD-oriented samples were smaller with a 12.6 mm length and a 5 mm width. The tensile properties were measured at room temperature at a strain rate of 10^{-3}s^{-1} using a Zwick Z100 (for the LD samples) and a Instron 5582 (for the TD samples) universal tensile testing machine. The three point bending test was carried out according to the ISO7438 standard. The sample size for the bending tests was 20 mm × 60 mm. The punch speed was 20 mm min^{-1} and the diameter of the two rollers on either side of the central punch was 40 mm.

The fractography of the Zn-coated PHS bending speci-

mens was carried out in a ZEISS Ultra 55 Field Emission Scanning Electron Microscopy (FE-SEM). The cross-sectional coating structure was analysed in specific areas on the inside and the outside of the die-quenched part as shown in Fig. 2. The microstructure observations were carried out with a JEOL JXA-8530F Field Emission Electron Probe Micro-Analyser (FE-EPMA) and elemental distributions were obtained by Wavelength Dispersive Spectroscopy (WDS). The elemental mapping was used to track the sub-surface liquid metal penetration in the steel substrate. An FEI QUANTA 3D was used for Transmission Electron Microscopy (TEM) sample preparation using the Focussed Ion Beam (FIB) thinning method. The microstructural analysis was carried out in a JEOL JEM-2100F Field Emission Transmission Electron Microscope (FE-TEM) and the samples were analysed by Selected Area Diffraction (SAD) and Energy Dispersive Spectroscopy (EDS).

3. Results

Figure 3 shows the uniaxial tensile engineering stress-engineering strain curves for the die-quenched uncoated and Zn-coated PHS. The tests were done with specimens from two different areas, *i.e.* the top and wall segments of the part, and in two directions, *i.e.* the LD and TD directions. All of the tested specimen had a YS in the range of 1 000–1 100 MPa, and UTS in the range of 1 400–1 500 MPa. The total elongation (TE) was 6–8% for the LD samples and 10–12% for the TD samples. The variation of the TE in samples taken in the same direction was very small. The difference in TE and post-uniform elongation between LD and TD-oriented samples was much larger. This is mainly due to the specimen size, the TD-oriented samples being much shorter than the LD-oriented samples with same thickness. The top part, which was less deformed than the wall part, had similar properties in terms of YS, UTS and TE. The results show clearly (a) that the Zn coating has a negligible influence on the tensile properties after die-quenching and (b) that the tensile properties of the die-quenched PHS are homogeneous.

In contrast, the bending performance of the die-quenched PHS specimens were clearly different as shown in **Fig. 4**. The bendability of the various samples taken from the uncoated die-quenched PHS part were similar in terms of the bending angle at the maximum bending force F_{max}. The angles were 81.25° for the top sample and 78.77° for the wall sample taken in the LD-oriented samples, and 77.24°

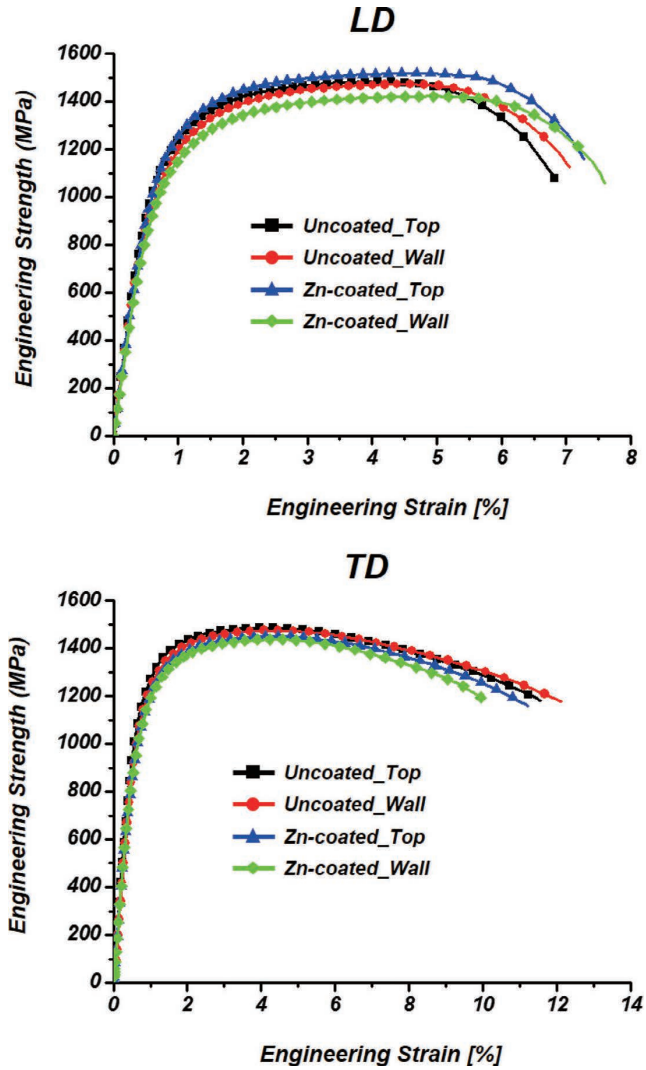

Fig. 3. Engineering stress-strain curves of the LD and TD oriented tensile specimens taken from the uncoated and Zn-coated die-quenched 22MnB5 PHS.

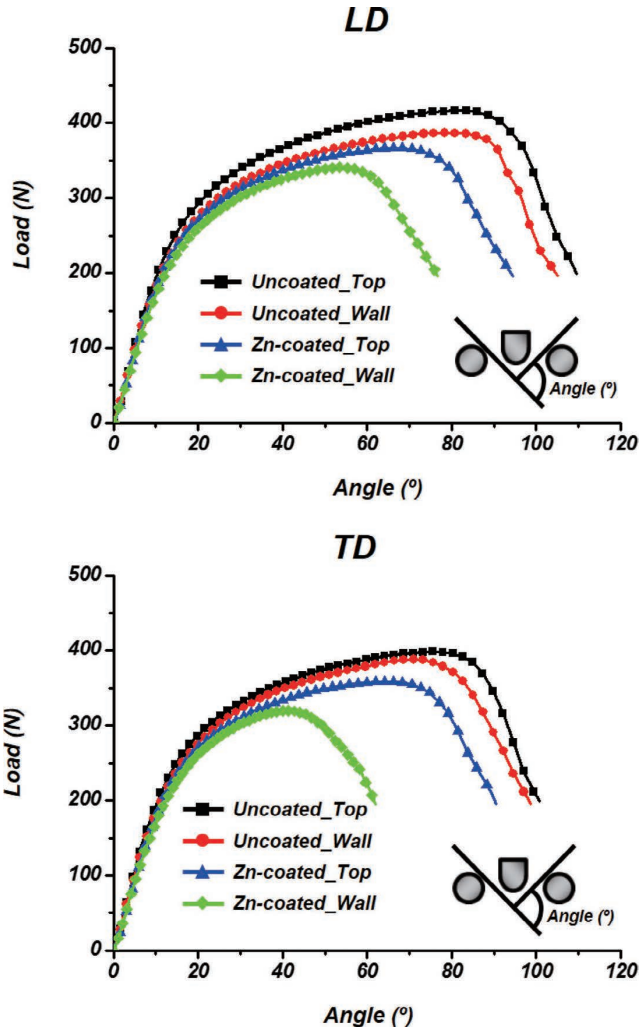

Fig. 4. Bending load versus bending angle curves of LD and TD oriented specimens taken from the uncoated and Zn-coated die-quenched PHS.

for the top sample and 72.09° for the wall sample, taken in the TD-orientation. The angle differences for different testing directions and different sample locations were about 5°. In the case of the Zn-coated die-quenched PHS part however, the angles were only 67.54° for a sample taken from the top and 54.27° for a sample taken from the wall area taken in the LD-orientation. The Zn-coated PHS samples oriented along the TD direction had an angle at maximum force of 66.09° for a sample taken from the top area and 41.47° for a sample taken from the wall. This corresponds to a difference related to the test sample location of about 13° in the LD-direction and angle reduction of 25° for samples taken from the wall. The Zn coating had clearly a significant effect on the bending performance of the die-quenched PHS parts. The bending performance of the die-quenched Zn-coated PHS samples taken from the wall area were worse than for samples taken from the top area. The lowest bendability was for samples taken in the wall area and oriented in the TD-direction, *i.e.* parallel to punching direction. The mechanical properties of uncoated and Zn-coated PHS are listed in **Table 1**.

The lower bending performance of the die-quenched Zn-coated PHS parts relative to the die-quenched uncoated PHS parts was in part due to the decarburization of uncoated PHS. Choi *et al*. reported that during heating an uncoated 22MnB5 PHS grade developed a 30 μm thick decarburized layer at its surface which was composed of a ferrite matrix with a small volume fraction of martensite islands and that the effect of the decarburization on the microstructure reached a depth of 55 μm. The presence of this decarburized layer resulted in a significant improvement of the bendability.[19] In the presence of a coating, the steel is protected from oxidation and decarburization during the austenitizing heat treatment, and the steel can develop a fully martensitic microstructure upon cooling.

Figure 5 shows the fracture surface of three Zn-coated PHS samples after the bending test. In the specimen taken from the top area, the fracture mode at the surface consisted of intergranular fracture in the alloy layer and ductile fracture in the steel matrix. In the specimen taken from the wall area, the fracture mode of samples oriented in the TD-direction intergranular fracture of the alloy layer was observed. This intergranular fracture mode continued to a depth of 30 μm in the steel matrix, which fractured in a ductile manner. The fracture surface for the specimen taken in the wall area in the LD-direction, *i.e.* perpendicular to the major forming strain direction, was composed of an intergranular fracture in the surface alloy layer and a ductile fracture in the steel matrix. In addition, there were microcracks approximately 20 μm in size under the Zn alloy layer. The integranular fracture could be clearly observed inside the cracks. From the fractography sample taken in the wall area and oriented in the TD-direction it is clear that the microcrack propagated along the prior austenite grain boundaries (PAGB). The fractured surface had a characteristic roughness due to the $\gamma \rightarrow \alpha'$ martensite transformation which takes place during the die-quenching. The microcracks were

Table 1. Tensile and bending properties of uncoated (CR) and Zn coated (Zn) 22MnB5 PHS.

		YS [MPa]	UTS [MPa]	TE [%]	F_{max} [N]	$Angle_{max}$ [°]
LD	CR_Top	1 108	1 484	6.83	416.5	81.25
	CR_Wall	1 026	1 473	7.05	386.7	78.77
	Zn_Top	1 133	1 519	7.27	366.6	67.54
	Zn_Wall	1 031	1 422	7.60	340.6	54.27
TD	CR_Top	1 136	1 486	11.57	398.2	77.24
	CR_Wall	1 121	1 475	12.13	387.9	72.09
	Zn_Top	1 082	1 451	11.22	358.5	66.09
	Zn_Wall	1 069	1 438	10.00	319.8	41.47

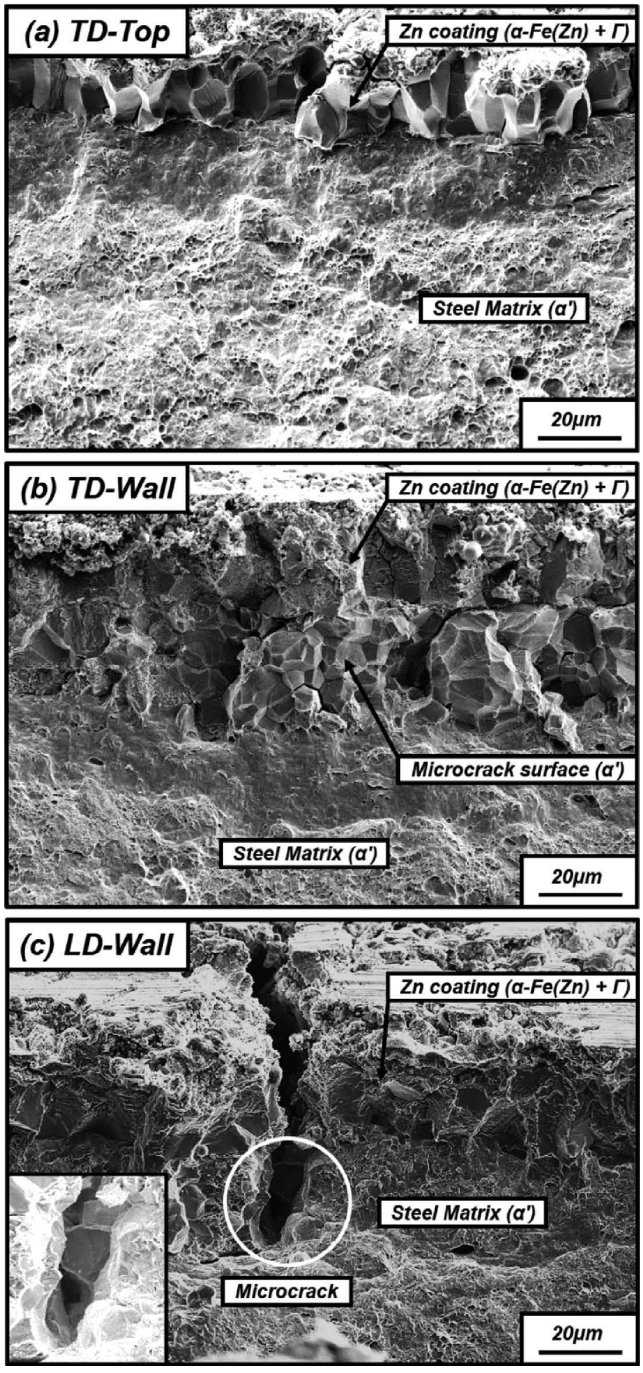

Fig. 5. SEM micrographs of the fracture surface after the bending test of the die-quenched Zn-coated 22MnB5 PHS for (a) the TD oriented sample from the top area, (b) the TD oriented sample taken from the wall area and (c) the LD oriented sample taken from the wall area.

therefore formed during press hardening, *i.e.* prior to the bending test.

A detailed cross sectional analysis of the specific areas of the press hardened Zn-coated 22MnB5 was carried out to investigate the origin of the microcracks. **Figure 6** shows the Fe and Zn elemental distribution on cross sections of die-quenched Zn-coated PHS in the seven specific areas labelled 1 to 7 in Fig. 2. After the press hardening process, the surface alloy consisted of the Γ-Fe_3Zn_{10} Fe–Zn intermetallic compound between coarse grains of α-Fe(Zn), *i.e.* α-Fe with Zn in solid solution. The top surface (1) was not deformed and the coating did not contain any cracks. The surface of the top inner corner (3) and the bottom corner outer surface (6) were deformed in compression but no coating cracks were observed. The surface of the top outer corner (2) and the bottom inner corner (7) were deformed in tension. The surface alloy layer contained intergranular cracks on α-Fe(Zn) grain boundaries. The wall outer surface (5) showed microcrack propagation from the alloy surface layer into the steel substrate while the inner wall surface (6) had clear cracks. The outer wall surface was initially deformed by compression in bending and then deformed in tension during unbending, and finally strained longitudinally. During the bending-unbending deformation, a friction shear stress was applied on the outer surface while the inner surface was not subject to any friction because only the outer surface made direct contact with the forming die. The deformation path for the wall material is illustrated in **Fig. 7**. The microcracks on the outer wall propagated intergranularly along austenite grain boundaries as shown in **Fig. 8**.

At the tip of the microcrack, the presence of Zn was clearly observed as shown in Fig. 6. For the present study, a FE-TEM specimen was prepared by the focused ion beam (FIB) method in the area where the liquid Zn penetrated. **Figure**

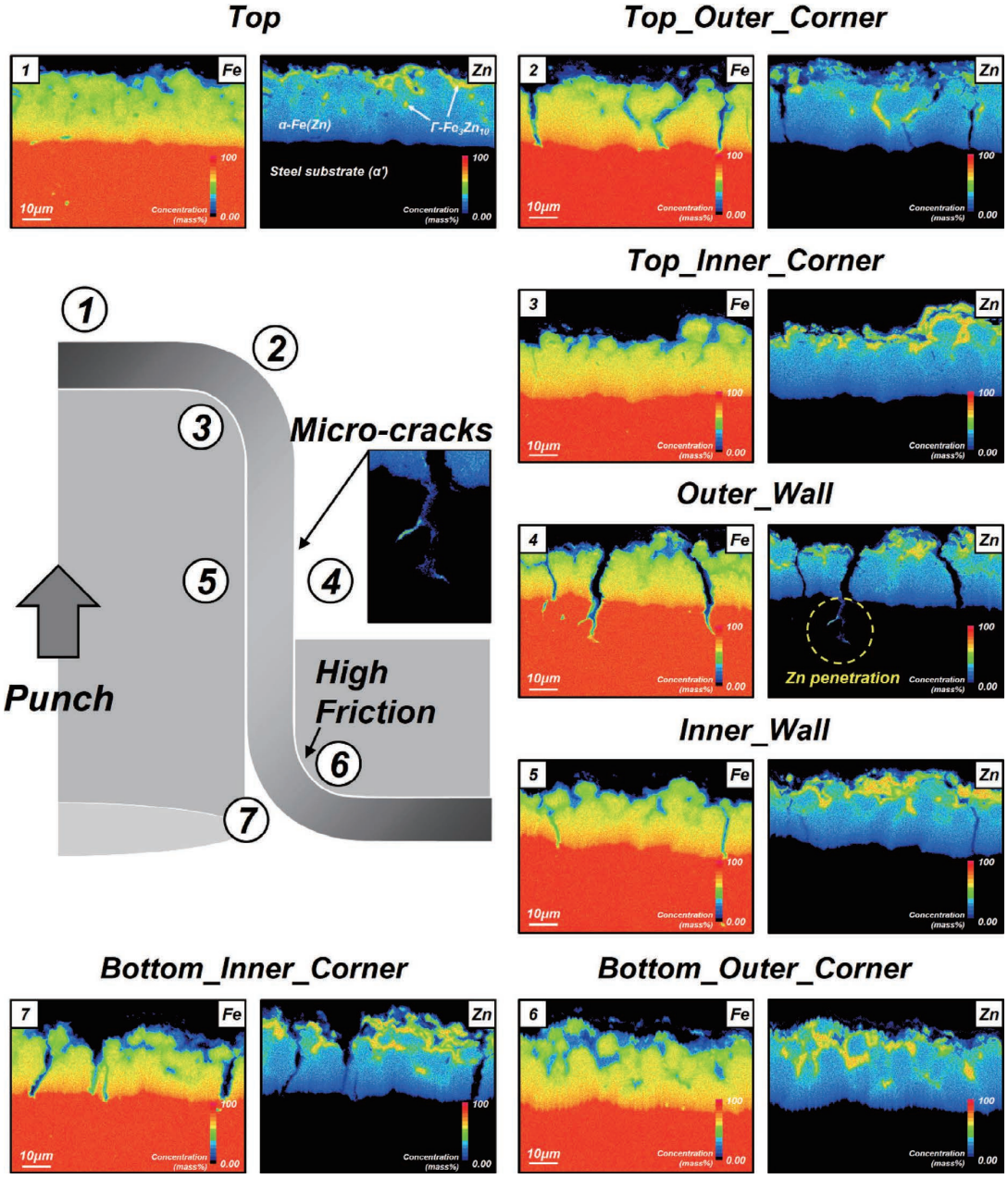

Fig. 6. Cross sectional view of the Fe and Zn elemental distribution of the Zn-coated 22MnB5 PHS die-quenched part for the areas defined in Fig. 2.

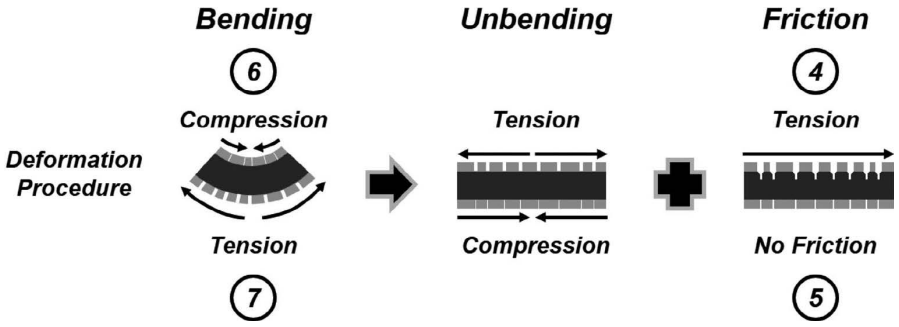

Fig. 7. Schematic of the deformations and the stresses applied during LMIE microcrack propagation in the die-quench press forming process.

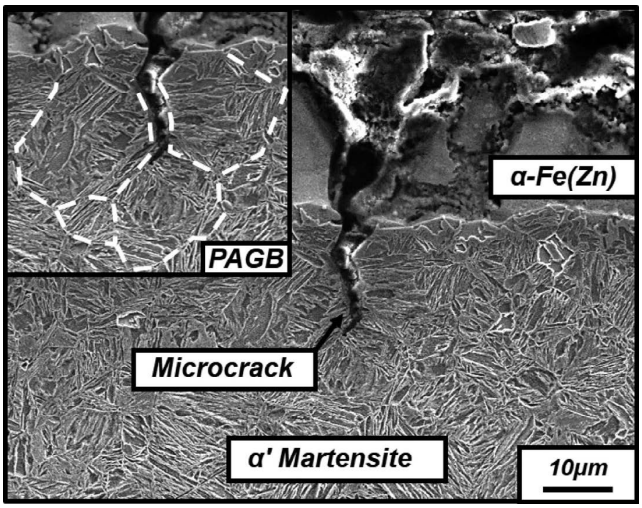

Fig. 8. SEM cross-sectional micrographs showing the LMIE microcrack propagation along prior austenite grain boundaries in die-quenched Zn-coated 22MnB5 PHS.

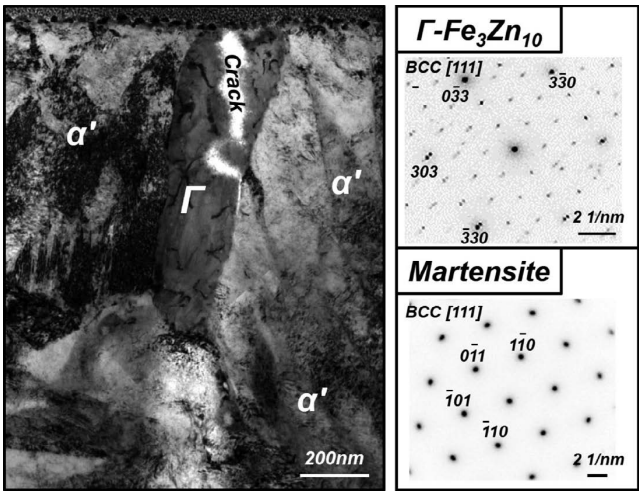

Fig. 9. TEM micrograph and corresponding diffraction patterns of the liquid Zn penetration area at the tip of a LMIE microcrack.

9 shows a TEM micrograph and the corresponding selected-area diffraction patterns (SADP). The precise location of the high temperature penetration of the liquid Zn can be observed at room temperature as it transforms to the Γ-Fe_3Zn_{10} Fe–Zn intermetallic compound upon cooling and solidification. The SADP of the Γ-Fe_3Zn_{10} corresponds to the BCC [111] zone axis and the α' martensite image is take close to the corresponding to the BCC [111] zone axis. **Figure 10** shows an EDS line profile across the Γ-Fe_3Zn_{10} and the Fe and Zn elemental distribution at the microcrack tip. The line profiles show an approximately 200 nm thick Γ-Fe_3Zn_{10} layer containing about 80 wt.% of Zn. There were two narrow Zn penetration zones less than 50 nm in width below this Γ-Fe_3Zn_{10} phase. This was identified as a thin intergranular layer of α-Fe(Zn) containing 30 wt.% of Zn.

4. Discussion

Two conditions for must be met to observe LMIE cracks in die-quenched Zn-coated PHS: (1) liquid Zn metal should be in direct contact with the steel substrate and (2) the applied stress should exceed a critical value.[8,20] In the present study, the die-quenched Zn coating on the PHS was composed of Γ-Fe_3Zn_{10} and α-Fe(Zn). The Zn concentration of Γ-Fe_3Zn_{10} and α-Fe(Zn) phases was about 80 wt.% and 30 wt.%, respectively. During the heating stage of the press hardening heat treatment, the original pure Zn coating was changed to a mixture of α-Fe(Zn) and Γ-Fe_3Zn_{10} which was solid up to the peritectic transformation temperature of 782. At the peritectic temperature, the solid Γ-Fe_3Zn_{10} transforms to Fe-saturated liquid Zn and solid α-Fe(Zn). The room temperature distribution of the Γ-Fe_3Zn_{10} phase corresponds therefore to the distribution of the liquid Zn during the press hardening heat treatment. The solidification temperature of Γ-Fe_3Zn_{10} is close to typical forming temperatures (750°C) during the die-quenching. The micro crack region included coating cracks and their propagation as LMIE microcracks into the steel which occurred in the areas where the specimen was subject to tension. The LMIE microcracks were only present on the outer wall surface where the specimen was subject to sufficiently high stresses due to a combination of large tensile stresses and additional shear stresses caused by friction.

Different models for LMIE-related intergranular crack formation mechanism have been proposed: the dissolution-diffusion based models,[21,22] the brittle fracture model,[23] the ductile fracture model,[24,25] the liquid metal penetration model[26] and the bilayer interfacial phase fracture model.[27] In the present case, the LMIE by liquid Zn shares some features with previously proposed models. A new LMIE model is however proposed, which takes into account the specifics of the LMIE microcrack structure observed on die-quenched PHS parts. The mechanism consists of four stages:

Stage 1. The Zn diffusion in the austenite grain boundaries.

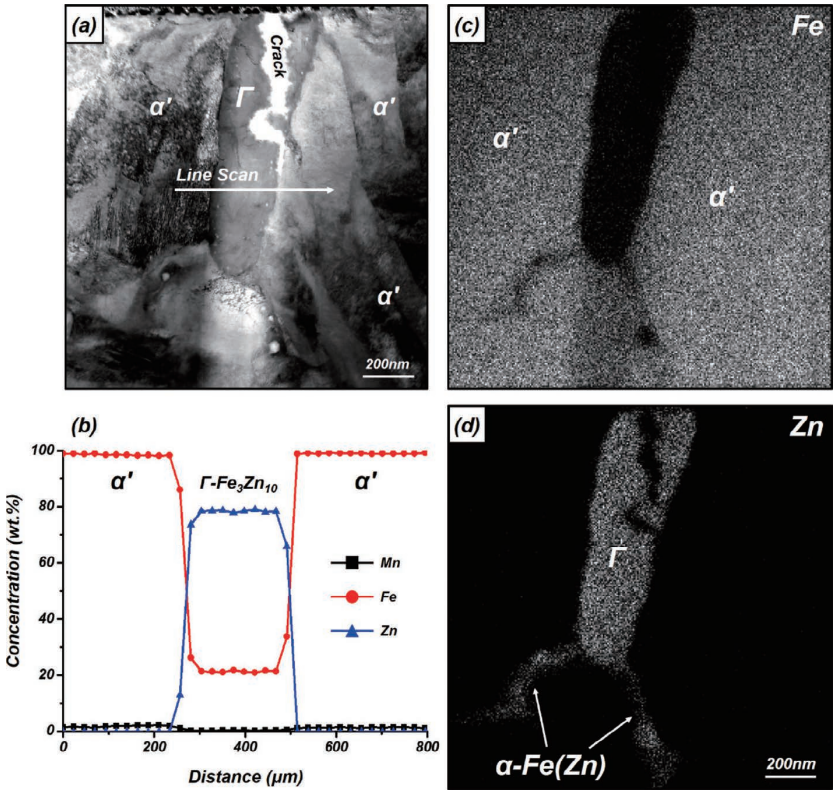

Fig. 10. (a) STEM micrograph and (b) corresponding EDS depth profile of the same region as Fig. 9. The elemental distribution for (c) Fe and (d) Zn in the Zn penetration area at the tip of the LMIE microcrack.

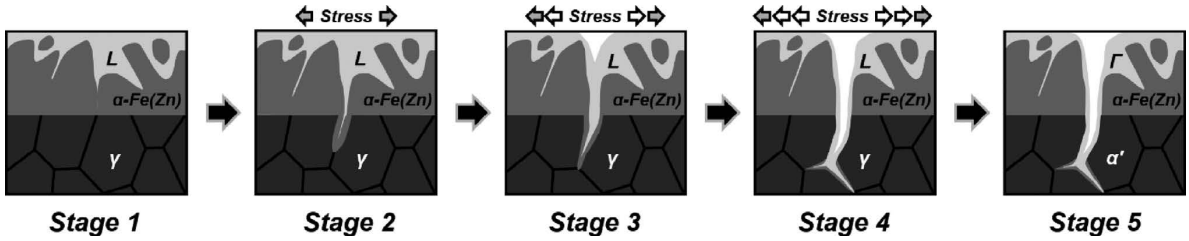

Fig. 11. The schematic of mechanism for LMIE microcrack on Zn-coated 22MnB5 PHS.

Stage 2. The diffusion of Zn from the austenite grain boundary region into the surrounding austenite matrix.

Stage 3. The austenite-to-ferrite transformation of the grain boundary region driven by the Zn diffusion in austenite, due to the low solubility of Zn in austenite.[28)]

Stage 4. The intergranular cracking of the boundary region, which has transformed to ferrite α-Fe(Zn), when an external stress is applied.

The thin α-Fe(Zn) grain boundary layer is easily be formed and it is prone to cracking for the following reasons: crack as (a) the Zn diffusion is faster in ferrite than in austenite, (b) Zn is a strong ferrite stabilizer,[11,29)] and (c) the strength and the strain hardening of ferrite are lower than for austenite at the allotropic transformation temperature.[30,31)]

The model is summarized in the schematic shown in **Fig. 11**. Before deformation, there is no Zn penetration (Stage 1). During the deformation under tension, the liquid Zn is in direct contact with the steel matrix and penetrated into the PAGBs. The austenite in the grain boundary region transformed to ferrite by Zn diffusion (Stage 2). The crack was initiated in the α-Fe(Zn) boundary phase and it propagated along PAGBs. The crack continued to be filled with liquid Zn due to capillary forces (Stage 3). This process continues until the applied stress was removed. The room temperature observation of Γ-Fe_3Zn_{10} at the crack tip makes it possible to observe the extension of the liquid Zn penetration at high temperature (Stage 4). The liquid Zn transforms to Γ-Fe_3Zn_{10} and the austenite transforms to the martensite after die-quenching (Stage 5).

In order to avoid LMIE microcrack formation, the diffusion Zn in the austenite boundaries during the die-quenching should be avoided. Lee *et al.*[8)] suggested that the annealing treatment could be carried out at higher temperature, for longer soaking times or that a thinner coating layer could be used. Higher heating temperatures provide a faster Zn diffusion in the matrix and the formation of a surface alloy layer consisting entirely of α-Fe(Zn) with no Γ-Fe_3Zn_{10}. Longer soaking times have the same outcome obtained by means of a longer diffusion time. The use of thinner coatings reduces the amount of Zn which needs to be dissolved to form α-Fe(Zn). The effect of the soaking time and the coating thickness or weight on LMIE and microcrack propagation has been reported previously and the reduction of the susceptibility to LMIE and microcrack propagation with increased soaking times or reduced coating weights has also been reported.[8,32–35)] It is expected that a reduction of the

applied stress during press hardening process should also be beneficial. The area most vulnerable to LMIE microcrack formation is the outer wall. The stress causing LMIE is partially due to friction in this area. The friction coefficient of PHS during the die forming process is higher than in conventional press forming at room temperature. Zn and Zn-alloy coatings including Zn–Ni coating provide a lower friction coefficient than the Al–Si coating on PHS.[36,37] This lower friction is however not sufficiently low to suppress LMIE microcrack propagation. There are various solutions to further reduce the friction: the increase of the die radius, the surface treatment of the tools and the use of a lubricant. Kim *et al*. reported that the microcrack propagation was significantly suppressed when the die radius was increased and the plastic strain limited.[35] Bachmann *et al*. reported that a nitriding surface treatment could decrease the friction coefficient for Zn and Zn-alloy coated PHS.[37] The use of lubricant has also been reported as an effective method to decrease both friction and die wear.[38,39]

5. Conclusion

The mechanical properties of uncoated and Zn-coated die-quenched 22MnB5 PHS parts were evaluated in terms of tensile properties and bending performance. The better bendability observed for the die-quenched uncoated PHS was mainly caused by the surface decarburization. For the die-quenched Zn-coated PHS, the bending performance was sensitive to the sample orientation and the position of the sample in the part, *i.e.* whether the sample was taken from the top or the wall of the part. The tensile properties did not significantly depend on these conditions. The bending properties of the outer wall side in the TD-orientation were deteriorated due to microcracking. TD-oriented samples provided a poor bendability compared to LD-oriented samples because the bending direction of the TD-oriented samples coincided with the microcrack propagation direction. The origin of the microcracks was identified as LMIE by liquid Zn. The LMIE occurred when an Fe-saturated liquid Zn phase was present during the die-quenching and a sufficiently high stress was applied. The Γ-Fe_3Zn_{10} Fe–Zn intermetallic compound was present at the microcrack tip at room temperature. This phase was formed from the liquid Zn phase during the cooling after the press hardening process. The LMIE microcracks formed only at the outer wall surface of the Zn-coated PHS. During the press hardening process, the outer wall surface is subject to both frictional stresses and tensile stresses. The LMIE microcracks propagated intergranularly along prior austenite grain boundaries. A mechanism for the LMIE of Zn-coated PHS was proposed. In this mechanism, a thin α-Fe(Zn) layer is formed at the prior austenite grain boundaries as a result of the phase transformation of the austenite grain boundary area by the Zn diffusing preferentially along the austenite grain boundaries. Ferrite, which has a low strength and a lower strain hardening compared to the fracture of the austenite boundary during the die-forming. The LMIE microcrack problem can be alleviated by diffusion annealing treatments which reduce or eliminate the liquid Zn by replacing it with a solid solution of Zn in ferrite. Tool surface treatment, such as nitriding, and the use of lubricants can decrease friction during forming and contribute to the elimination of crack formation.

REFERENCES

1) K. Steinhoff, N. Barbakadze and M. Schupfer: 8th Int. Conf. on Zinc and Zinc Alloy Coated Steel Sheet, AIM, Milano, (2011), 319.
2) J. Lee, S. -J. Lee and B. C. De Cooman: *Mater. Sci. Eng. A*, **536** (2012), 231.
3) J. P. Kong, T. K. Han, K. G. Chin, B. G. Park and C. Y. Kang: *Mater. Design*, **54** (2014), 598.
4) S. Lee, S.-J. Lee and B. C. De Cooman: *Acta Mater.*, **59** (2011), 7546.
5) S. Lee, J. Kim, S.-J. Lee and B. C. De Cooman: *Scr. Mater.*, **65** (2011), 528.
6) H. Karbasian and A. E. Tekkaya: *J. Mater. Process. Technol.*, **210** (2010), 2103.
7) K. Mori, K. Akita and Y. Abe: *Int. J. Mach. Tool. Manuf.*, **47** (2007), 321.
8) C. W. Lee, D. W. Fan, I. R. Sohn, S. J. Lee and B. C. De Cooman: *Metall. Mater. Trans. A*, **43** (2012), 5122.
9) M. Windmann, A. Röttger and W. Theisen: *Surf. Coat. Technol.*, **246** (2014), 17.
10) D. W. Fan, R. B. Park, Y. R. Cho and B. C. De Cooman: *Steel Res. Int.*, **81** (2010), 292.
11) B. C. De Cooman and J. G. Speer: Fundamentals of Steel Product Physical Metallurgy, 1st ed., AIST, Warrendale, PA, (2011).
12) A. Bardelcik, C. P. Salisbury, S. Winkler, M. A. Wells and M. J. Worswick: *Int. J. Impact Eng.*, **37** (2010), 694.
13) C. Alléy, L. Dosdat, O. Clauzeau, K. Ogle and P. Volovitch: *Surf. Coat. Technol.*, **238** (2014), 188.
14) R. Autengruber, G. Luckeneder and A. W. Hassel: *Corros. Sci.*, **63** (2012), 12.
15) J. Kondratiuk. P. Kuhn, E. Labrenz and C. Bischoff: *Surf. Coat. Technol.*, **205** (2011), 4141.
16) P. Drillet, R. Grigorieva, G. Leuillier and T. Vietoris: 8th Int. Conf. on Zinc and Zinc Alloy Coated Steel Sheet, AIM, Milano, (2011), 371.
17) L. Till and P. Markus: 1st Int. Conf. Hot Sheet Metal Forming of High-performance Steel, CHS^2, Kassel, (2008), 143.
18) M. Manuel, C. Jorg, S. Monika, K. Steffen, A. Michael and S. Kurt: 3rd Int. Conf. Hot Sheet Metal Forming of High-performance Steel, CHS^2, Kassel, (2011), 49.
19) W. S. Choi and B. C. De Cooman: *Steel Res. Int.*, **85** (2014), 824.
20) M. G. Nicholas and C. F. Old: *J. Mater. Sci.*, **14** (1979), 1.
21) W. M. Robertson: *Trans. Met. Soc. AIME*, **236** (1966), 1478.
22) E. E. Glickman and Y. V. Goryunov: *Sov. Mater. Sci.*, **14** (1978), 355.
23) M. H. Kamdar: Treatise on Materials Science and Technology, Vol. 25, ed. by C. L. Briant and S. K. Banerji, Academic Press, New York, (1983), 361.
24) S. P. Lynch: *Mater. Charact.*, **29** (1992), 279.
25) V. V. Popovich: *Fiz.-Khim. Mekh. Mater.*, **5** (1979), 11.
26) P. Gordon: *Metall. Trans. A*, **9A** (1978), 267.
27) J. Luo, H. Cheng, K. M. Asl, C. J. Kiely and M. P. Harmer: *Science*, **333** (2011), 1730.
28) X. Su, N.-Y. Tang and J. M. Toguri: *J. Alloys Compd.*, **325** (2001), 129.
29) H. Oikawa: *Tech. Rep., Tohoku Univ.*, **47** (1982), 215.
30) H. G. Suzuki, S. Nishimura, J. Imamura and Y. Nakamura: *Trans. Iron Steel Inst. Jpn.*, **24** (1984), 177.
31) D. J. Seol, Y. M. Won, T. Yeo, K. H. Oh, J. K. Park and C. H. Yim: *ISIJ Int.*, **39** (1999), 91.
32) L. A. Reini, M. Choi and A. Wendorf: 4th Int. Conf. Hot Sheet Metal Forming of High-performance Steel, CHS^2, Luleå, (2013), 223.
33) M. Takahashi, K. Akoika, H. Takebayashi, K. Imai, T. Yonebayashi, M. Nakata, T. Takayama and N. Kojima: 4th Int. Conf. Hot Sheet Metal Forming of High-performance Steel, CHS^2, Luleå, (2013), 453.
34) H. Schwinghammer, G. Luckenender, T. Manzenreiter, M. Rosner, P. Tsipouridis and T. Kurz: 4th Int. Conf. Hot Sheet Metal Forming of High-performance Steel, CHS^2, Luleå, (2013), 527.
35) S. Kim, I. Son, D. Kim and S. Kim: 4th Int. Conf. Hot Sheet Metal Forming of High-performance Steel, CHS^2, Luleå, (2013), 537.
36) J. Kondratiuk and P. Kuhn: *Wear*, **270** (2011), 839.
37) M. Bachmann, R. Fell and A. Ademaj: 4th Int. Conf. Hot Sheet Metal Forming of High-performance Steel, CHS^2, Luleå, (2013), 507.
38) A. Yanagida and A. Azushima: *CIRP Annals – Manuf. Technol.*, **58** (2009), 247.
39) A. Azushima, K. Uda and A. Yanagida: *J. Mater. Process. Technol.*, **212** (2012), 1014.